

The Negative Ion Photoelectron Spectrum of Cyclopropane-1,2,3-Trione Radical Anion, $(\text{CO})_3^{\bullet-}$ — A Joint Experimental and Computational Study

Bo Chen,[†] David A. Hrovat,[†] Robert West,[‡] Shihu H. M. Deng,[§] Xue-Bin Wang,^{*,§} and Weston Thatcher Borden^{*,†}

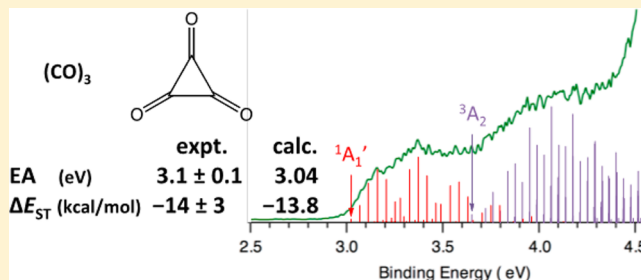
[†]Department of Chemistry and the Center for Advanced, Scientific Computing and Modeling, University of North Texas, 1155 Union Circle, #305070, Denton, Texas 76203-5070, United States

[‡]Department of Chemistry, University of Wisconsin, 1101 University Avenue, Madison, Wisconsin 53706, United States

[§]Physical Sciences Division, Pacific Northwest National Laboratory, P.O. Box 999, MS K8-88, Richland, Washington 99352, United States

Supporting Information

ABSTRACT: Negative ion photoelectron (NIPE) spectra of the radical anion of cyclopropane-1,2,3-trione, $(\text{CO})_3^{\bullet-}$, have been obtained at 20 K, using both 355 and 266 nm lasers for electron photodetachment. The spectra show broadened bands, due to the short lifetimes of both the singlet and triplet states of neutral $(\text{CO})_3$ and, to a lesser extent, to the vibrational progressions that accompany the photodetachment process. The smaller intensity of the band with the lower electron binding energy suggests that the singlet is the ground state of $(\text{CO})_3$. From the NIPE spectra, the electron affinity (EA) and the singlet–triplet energy gap of $(\text{CO})_3$ are estimated to be, respectively, EA = 3.1 ± 0.1 eV and $\Delta E_{\text{ST}} = -14 \pm 3$ kcal/mol. High-level, (U)CCSD(T)/aug-cc-pVQZ// (U)CCSD(T)/aug-cc-pVTZ, calculations give EA = 3.04 eV for the $^1A_1'$ ground state of $(\text{CO})_3$ and $\Delta E_{\text{ST}} = -13.8$ kcal/mol for the energy gap between the $^1A_1'$ and 3A_2 states, in excellent agreement with values from the NIPE spectra. In addition, simulations of the vibrational structures for formation of these states of $(\text{CO})_3$ from the $^2A_2''$ state of $(\text{CO})_3^{\bullet-}$ provide a good fit to the shapes of broad bands in the 266 nm NIPE spectrum. The NIPE spectrum of $(\text{CO})_3^{\bullet-}$ and the analysis of the spectrum by high-quality electronic structure calculations demonstrate that NIPES can not only access and provide information about transition structures but NIPES can also access and provide information about hilltops on potential energy surfaces.



INTRODUCTION

Recent interest in the oxocarbons, $(\text{CO})_n$, was initially stimulated by calculations on 1,2,3,4-cyclobutanetetraone, $(\text{CO})_4$.^{1,2} This cyclic tetraketone would, naively, be expected to have a closed-shell, singlet ground state. However, calculations by others¹ and by us² predicted that this molecule would, instead, have a triplet ground state. Subsequent negative ion photoelectron spectroscopy (NIPES) confirmed this prediction, that the ground state of $(\text{CO})_4$ is a triplet.³

On the other hand, $(\text{CO})_5$ and $(\text{CO})_6$ were each predicted to have a singlet ground state by both qualitative MO analysis and quantitative calculations.^{2c} Subsequent NIPES studies of $(\text{CO})_5^{\bullet-}$ and $(\text{CO})_6^{\bullet-}$ not only confirmed these predictions but also provided accurate electron affinities (EAs) and singlet–triplet energy differences (ΔE_{ST}) for $(\text{CO})_5$ and $(\text{CO})_6$.⁴ Additional calculations of the Franck–Condon factors (FCFs) for $(\text{CO})_n^{\bullet-} \rightarrow (\text{CO})_n$ for $n = 4-6$, led to successful simulations of the vibrational structures in all of the bands in the NIPE spectra of these three radical anions.⁴

We have used this three-step approach, (1) theoretical predictions \rightarrow (2) NIPES experiments \rightarrow (3) calculation-assisted interpretations of the NIPE spectra, to investigate the electronic structures of not only $(\text{CO})_n$ ($n = 4-6$)¹⁻⁴ but, more recently, of $(\text{CS})_4$ ⁵ and *meta*-benzoquinone (MBQ).⁶ The third step in this approach has proven to be indispensable when the observed NIPE spectra are very complicated, as is the case of MBQ.^{6b}

PREDICTIONS ABOUT $(\text{CO})_3$

The $n = 3$ member of the oxocarbons, $(\text{CO})_3$, has been the subject of several different computational studies.^{2c,7,8} Our qualitative MO analysis and our quantitative calculations^{2c} both predicted that $(\text{CO})_3$ has a closed-shell, singlet ground state, ($^1A_1'$), in which the e' set of oxygen lone-pair MOs is fully occupied and the a_2'' π MO is empty (Figure 1). Calculations at the (U)CCSD(T)/6-311+G(2df)//(U)-

Received: June 3, 2014

Published: August 22, 2014

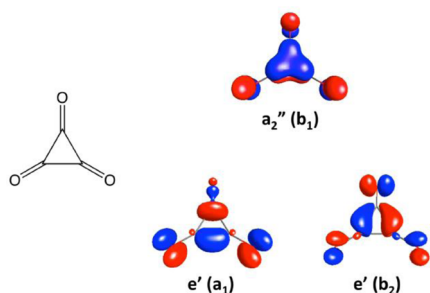


Figure 1. Frontier MOs of $(\text{CO})_3$. The symmetry label of each orbital is given for both D_{3h} and C_{2v} (in parentheses) geometries. In the lowest singlet state of $(\text{CO})_3$, the e' set of σ MOs is fully occupied and the a_2'' π MO is empty. In the lowest triplet state one electron is excited from an e' MO into the a_2'' MO.

B3LYP/6-311+G(2df) level of theory^{2c} predicted the lowest triplet state (${}^3E''$) of $(\text{CO})_3$, in which the a_2'' MO and one MO of the e' set are singly occupied, to be 26.5 kcal/mol higher in energy than the ${}^1A_1'$ ground state at the optimized D_{3h} geometries for these two states.

However, our calculations^{2c} found that a D_{3h} geometry is not the equilibrium geometry of either the singlet or the triplet state. A vibrational analysis found that the ${}^1A_1'$ ground state of $(\text{CO})_3$ has two imaginary frequencies, which correspond to a degenerate pair of e'' vibrations. These vibrations allow the high-lying, filled, e' MOs and the low-lying, empty, a_2'' MO to mix; and this orbital mixing makes the pathway to fragmentation of $(\text{CO})_3$ to three CO molecules calculated to be barrierless on the singlet potential energy surface. Thus, the lowest energy, D_{3h} geometry of the ${}^1A_1'$ ground state of $(\text{CO})_3$ is not predicted to be a minimum or even a transition structure on the singlet potential energy surface, but instead, this geometry is calculated to be a hilltop, with two negative second derivatives.

The D_{3h} geometry of the lowest energy triplet state of $(\text{CO})_3$ is also expected to be unstable to a symmetry-lowering pair of degenerate vibrations. This triplet state has E'' symmetry, and hence, it should undergo a first-order, Jahn–Teller stabilization on an e' molecular distortion.¹² Such a distortion can lead to a triplet $(\text{CO})_3$ molecule with C_{2v} symmetry and one short and two long C–C ring bonds (3A_2 electronic state) or two short and one very long C–C ring bond (3B_1 electronic state). The latter distortion is likely to relieve more strain in the three-membered ring than the former, so that 3B_1 is expected to lie below 3A_2 at their optimized C_{2v} geometries. Our previous calculations^{2c} found that the 3B_1 state of $(\text{CO})_3$ is 27.1 kcal/mol lower in energy than the undistorted ${}^3E''$ state at the (U)B3LYP/6-311+G(2df) level.

As shown schematically in Figure 2, the C_{2v} geometry of the 3B_1 state, with one very long and two short C–C bonds, could, quite possibly, undergo a further, antisymmetric C–C bond-length distortion, extruding a molecule of CO, with concomitant formation of the triplet ground state of $(\text{CO})_2$.¹³ However, depending on whether or not such a bond length distortion is barrierless, the 3B_1 diradicals, formed by Jahn–Teller distortion of the ${}^3E''$ state from D_{3h} symmetry, could be local minima on the triplet potential energy surface.

Although it might seem that continued lengthening of the two long bonds in the 3A_2 electronic state of $(\text{CO})_3$ would also lead to fragmentation to ${}^3(\text{CO})_2 + \text{CO}$, this is not the case. As shown in Figure 3, in ${}^3(\text{CO})_2$ the two unpaired electrons each

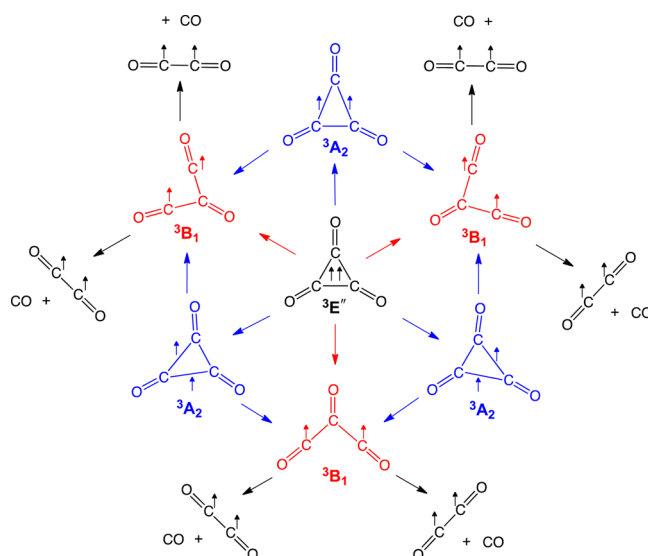


Figure 2. Depiction of the Jahn–Teller distortions¹² of the ${}^3E''$ state of D_{3h} $(\text{CO})_3$ to the C_{2v} geometries of the 3B_1 and 3A_2 components of this state. The 3B_1 diradicals are expected to be the energy minima and the 3A_2 diradicals the transition structures on the pseudorotation pathway about the conical intersection between 3B_1 and 3A_2 at D_{3h} geometries. The 3B_1 local energy minima could, as shown, undergo a further antisymmetric distortion of the C–C bond lengths, leading to extrusion of a molecule of CO, with concomitant formation of the triplet ground state of $(\text{CO})_2$.¹³ As discussed in the text, least motion fragmentation of 3A_2 to ${}^3(\text{CO})_2 + \text{CO}$ is forbidden by state symmetry.¹⁴

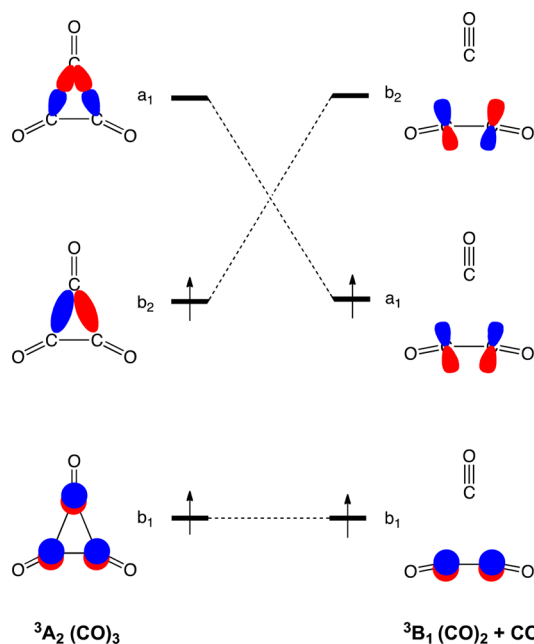


Figure 3. Schematic orbital correlation diagram for the concerted fragmentation of the 3A_2 state of $(\text{CO})_3$ to the 3B_1 state of $(\text{CO})_2$ plus CO along a C_{2v} pathway. The AOs on the oxygen atoms are omitted for clarity.

occupy a MO that is C–C bonding. In the C_{2v} point group, one of these singly occupied MOs has b_1 symmetry, and the other has a_1 symmetry, so the ground state of ${}^3(\text{CO})_2$ is 3B_1 in C_{2v} symmetry. Consequently, the fragmentation of the 3A_2 state of $(\text{CO})_3$ to the 3B_1 state of ${}^3(\text{CO})_2 + \text{CO}$ is forbidden by state

symmetry, because there is a crossing between a b_2 MO, which is singly occupied in the 3A_2 state of $(CO)_3$, and an a_1 MO, which is singly occupied in the 3B_1 ground state of $(CO)_2$.¹⁴

Since the least-motion fragmentation of the 3A_2 state of $(CO)_3$ to $^3(CO)_2 + CO$ is a forbidden reaction, fragmentation of the 3A_2 state of $(CO)_3$ requires antisymmetric distortion of the C_{2v} geometry of this state to the geometry of the 3B_1 state. As shown in Figure 2, there are two 3B_1 geometries that are adjacent to each 3A_2 geometry on the pathway for pseudorotation about the conical intersection between 3B_1 and 3A_2 , which occurs at D_{3h} geometries. As discussed above, the three 3B_1 geometries are anticipated to be local energy minima along the pseudorotation pathway, and the 3A_2 geometries are expected to be the transition structures that connect pairs of 3B_1 minima.

In the $(CO)_3^{\bullet-}$ radical anion, the unpaired electron is expected to occupy the a_2'' MO. Thus, unlike the case in the lowest singlet and triplet states of neutral $(CO)_3$, there is every reason to expect the equilibrium geometry of the $(CO)_3^{\bullet-}$ radical anion to have D_{3h} symmetry. Therefore, vertical electron loss from $(CO)_3^{\bullet-}$ in a NIPES experiment should form the lowest singlet state of neutral $(CO)_3$ at a geometry at which this state is expected to be unstable toward a pair of e'' molecular distortions away from D_{3h} symmetry.

Using NIPES to generate a neutral species at a geometry, where the state generated is a stationary point with one imaginary frequency, is called "transition state spectroscopy."¹⁵ However, formation of the lowest singlet state of $(CO)_3$ in a NIPES experiment on $(CO)_3^{\bullet-}$ would not really be transition state spectroscopy, because a D_{3h} geometry is a hilltop on the potential energy surface for the lowest singlet state. Therefore, a NIPES experiment on $(CO)_3^{\bullet-}$ provides an opportunity to test whether NIPES can be used for not only transition state spectroscopy but also for "hilltop spectroscopy".

On the potential energy surface for the lowest triplet state, a D_{3h} geometry is the vertex of a Jahn–Teller cone. Such a geometry is not even a stationary point, since it has two negative *first* derivatives. Based on our findings for the $^3E_2''$ state of $(CO)_3$ in our NIPES study of $(CO)_3^{\bullet-}$,⁴ it seemed likely that a NIPES experiment on $(CO)_3^{\bullet-}$ would access one or both of the C_{2v} Jahn–Teller-distorted geometries of neutral, triplet $(CO)_3$.

Since a D_{3h} geometry for the $^1A_1'$ ground state of $(CO)_3$ is expected to have two imaginary frequencies on the potential energy surface for the singlet, and since the Jahn–Teller-distorted, C_{2v} geometry of 3A_2 is expected to have one imaginary frequency on the potential surface for the triplet, it seemed likely that both states of $(CO)_3$ would be short-lived. If they were sufficiently short-lived, the bands for their formation would be broadened by the uncertainty principle, so that the bands might not be seen, or they might merge into one very broad band in the NIPE spectrum of $(CO)_3^{\bullet-}$. Therefore, it was with a mixture of excitement and trepidation that we set out to obtain the NIPE spectrum of $(CO)_3^{\bullet-}$.

■ NIPE SPECTROSCOPY OF $(CO)_3^{\bullet-}$

NIPE spectra were obtained by combining electrospray generation of $(CO)_3^{\bullet-}$ in the gas-phase with a temperature-controlled ion trap and a magnetic bottle time-of-flight (TOF) photoelectron spectrometer that was recently developed at PNNL.¹⁶ Fresh solutions for electrospraying were prepared in a N_2 glovebox by adding an aliquot of LiOH, dissolved in methanol, to a 10^{-3} M anhydrous methanolic solution of deltic

acid,¹⁷ followed by titration with a small amount of an acetonitrile solution of an electron-donor compound, tetrakis-(dimethylamino)ethylene (TDAE). Both $(CO)_3^{\bullet-}$ ($m/z = 84$) and $C_3O_3H^-$ ($m/z = 85$) ions were produced with about the same abundance. All anions generated by electrospray were guided by two RF-only quadrupoles and directed by a 90° ion bender into a 3-D cryogenic ion trap, where they were accumulated and thermalized via collisions with a cold background buffer gas (ca. 0.1 mTorr 20/80 H_2/He) for a period of 20–100 ms before being pulsed out into the extraction zone of a TOF mass spectrometer at a repetition rate of 10 Hz. In this work, the trap was operated at 20 K in order to achieve optimal instrument resolution as well as to eliminate vibrational hot bands of anions.

For each NIPES experiment, the ions of $(CO)_3^{\bullet-}$ were mass selected and decelerated before being intercepted by a probe laser beam from a Nd:YAG laser (266 nm, 4.661 eV; or 355 nm, 3.496 eV) in the photodetachment zone of the magnetic-bottle photoelectron analyzer. The laser was operated at a 20 Hz repetition rate with the ion beam off at alternating laser shots for shot-by-shot background subtraction. Photoelectrons were collected at nearly 100% efficiency by the magnetic bottle and analyzed in a 5.2 m flight tube. TOF photoelectron spectra were collected and converted to kinetic energy spectra, calibrated by the known spectra of I^- and ClO_2^- . The electron binding energy spectrum was obtained by subtracting the kinetic energy spectrum from the detachment photon energy used.

The best energy resolution obtainable for I^- and ClO_2^- , after full ion deceleration, was ca. 20 meV full width at half-maximum (fwhm) for 1 eV electrons. However, due to the modest intensity of the $(CO)_3^{\bullet-}$ ion beam and the light mass of $(CO)_3^{\bullet-}$, the current NIPES experiments were carried out with less optimal energy resolution of ca. 45 meV fwhm for 1 eV electrons and ca. 30 meV fwhm for 0.5 eV electrons, as estimated using the atomic I^- NIPE spectrum under similar conditions.

■ COMPUTATIONAL METHODOLOGY

The geometries of the electronic states of radical anion $(CO)_3^{\bullet-}$ and neutral $(CO)_3$ were initially optimized, using (U)B3LYP¹⁸ calculations with the 6-31G(d) basis set.¹⁹ The results of these (U)B3LYP calculations are provided in the Supporting Information for this article. All DFT calculations were carried out with the Gaussian 09 program.²⁰

Geometries were reoptimized, and vibrational analyses at these geometries were performed with (U)CCSD(T)²¹ calculations, using the aug-cc-pVTZ basis set.²² In order to obtain more accurate energetics, single-point energies at each optimized geometry were computed, again using the (U)CCSD(T) method but with the larger aug-cc-pVQZ²² basis set. These (U)CCSD(T) calculations were carried out with the MOLPRO 2010 program.²³

In order to simulate the vibrational structure in the NIPE spectrum of $(CO)_3^{\bullet-}$, the optimized geometries, harmonic vibrational frequencies, and normal mode vectors, obtained from the (U)CCSD(T)/aug-cc-pVTZ calculations, were used as input to the ezSpectrum (version 3.0) program.²⁴ Duschinsky rotation²⁵ was included in using ezSpectrum to calculate the Franck-Condon factors (FCFs)²⁶ for electronic transitions from the lowest electronic state of the radical anion $(CO)_3^{\bullet-}$ to each of the low-lying electronic states of neutral

(CO)₃. The calculated FCFs were then used to simulate the vibrational structure in the NIPE spectrum of (CO)₃^{•-}.

Simulations of the vibrational structure in the NIPE spectrum of (CO)₃^{•-}, using (U)B3LYP/6-31G(d) calculations, were also performed. The (U)B3LYP/6-31G(d) simulations are similar in appearance to the simulations obtained from the (U)CCSD(T)/aug-cc-pVTZ calculations. The (U)B3LYP/6-31G(d) simulations are shown in the Supporting Information.

RESULTS AND DISCUSSION

The NIPE Spectra of (CO)₃^{•-}. The low-temperature (20 K) NIPE spectra of (CO)₃^{•-}, obtained with 355 and 266 nm lasers, are shown in Figure 4. The bands in both spectra are very broad, and no well-resolved vibrational structure can be identified in either spectrum.

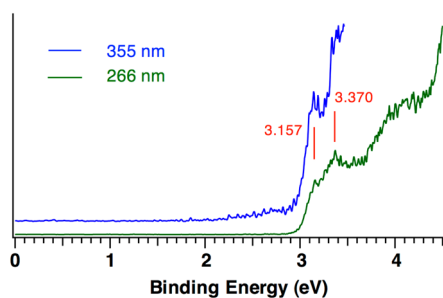


Figure 4. Low-temperature (20 K) NIPE spectrum of (CO)₃^{•-}, obtained with 355 nm (blue) and 266 nm (green) lasers.

As discussed in the introduction, the ¹A₁' and the ³A₂ states of (CO)₃ are likely to be short-lived. The ¹A₁' state is expected to fragment without a barrier to three molecules of CO, and the ³A₂ state is anticipated to undergo barrierless pseudorotation to the ³B₁ state. The latter state might fragment, without a barrier, giving ³(CO)₂ + CO. Hence, ³B₁ could also be very short-lived. Therefore, the observation of broadening in the low-energy bands in the NIPE spectrum of (CO)₃^{•-} is not at all surprising. However, our simulations, which are discussed in subsequent sections, reveal that the broadness of the spectra is due not only to the short lifetimes of the ¹A₁' and ³A₂ states of (CO)₃ but also to the extensive vibrational excitations that accompany electron photodetachment from (CO)₃^{•-}.

The 355 nm NIPE spectrum in Figure 4 shows what appear to be two maxima at electron binding energy (EBE) of ~3.16 and ~3.37 eV. The 266 nm spectrum exhibits two well-defined peaks on top of these two broad maxima, from which accurate EBEs of 3.157 ± 0.005 and 3.370 ± 0.005 eV are obtained. The 266 nm spectrum also shows a third broad band at EBE = 3.6–4.4 eV and a rising tail at EBE > 4.4 eV.

Both the 355 and 266 nm spectra of (CO)₃^{•-} show an onset at EBE ≈ 3.00 eV. Therefore, 3.00 eV can be regarded as the lower limit of EA of neutral (CO)₃. The apparent maximum at EBE = 3.157 eV could probably serve as an upper limit to the EA of neutral (CO)₃. However, we adopt a slightly more conservative value of EA = 3.1 ± 0.1 eV.

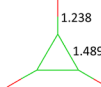


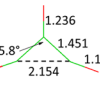

The second maximum in the NIPE spectrum, which occurs at EBE = 3.370 eV, could either be part of a vibrational progression that includes the maximum at EBE = 3.157 eV, or the maximum at EBE = 3.370 eV could be attributable to formation of the lowest triplet state. However, as discussed in a subsequent section, the simulation of the vibrational structure in the band for formation of singlet (CO)₃ strongly favors the first interpretation.

If the second maximum in the NIPE spectra in Figure 4 is provisionally assigned to a vibrational progression in the singlet, the third maximum at EBE = 3.6–4.4 eV in the 266 nm spectrum presumably belongs to the lowest triplet state of (CO)₃. Since a triplet state has three components, bands for formation of a triplet are usually more intense than those for formation of a singlet state.²⁷ Thus, the significantly greater integrated intensity of the band associated with the third maximum, compared to the band associated with the first two, is consistent with our prediction that a singlet should be the ground state of (CO)₃ and the triplet the first excited state.^{2c}

If we tentatively assign the valley at EBE ≈ 3.7 ± 0.1 eV in the 266 nm spectrum to be the onset of the band for the triplet and compare its energy with the estimate of 3.1 ± 0.1 eV for the energy of the onset that leads to the maximum EBE = 3.157 eV, we obtain a very rough experimental estimate of the singlet–triplet energy gap in (CO)₃ as ΔE_{ST} = -0.6 ± 0.14 eV = -14 ± 3 kcal/mol.

Calculations of the Energies of the Electronic States of (CO)₃^{•-} and (CO)₃. The analysis of the NIPE spectrum in the previous section leads to experimental estimates of EA = 3.1 ± 0.1 eV and ΔE_{ST} ≈ -14 ± 3 kcal/mol for (CO)₃. In order to

Table 1. (U)CCSD(T)/aug-cc-pVTZ Geometries and (U)CCSD(T)/aug-cc-pVQZ Energies, with (U)CCSD(T)/aug-cc-pVTZ Zero-Point Vibrational Energy Corrections, of the Electronic States of (CO)₃^{•-} and (CO)₃^a

	<i>D</i> _{3h} radical anion	<i>D</i> _{3h} singlet	<i>D</i> _{3h} triplet ^a	Jahn-Teller distorted <i>C</i> _{2v} triplet	
bond distances in Å					
electronic state	² A ₂ ^{•-}	¹ A ₁ '	³ E ^{•-}	³ B ₁	³ A ₂
orbital occupancy	...(e') ⁴ (a ₂) ¹	...(e') ⁴ (a ₂) ⁰	...(e') ³ (a ₂) ¹	...(a ₁) ¹ (b ₂) ² (b ₁) ¹	...(a ₁) ² (b ₂) ¹ (b ₁) ¹
calculated energy in kcal/mol	0	70.2	97.1	74.6	84.0
calculated energy in eV	0	3.04	4.21	3.24	3.64
experimentally estimated EBE in eV		3.1 ± 0.1			3.7 ± 0.1

^aThe calculated energies are compared with the experimental values from the NIPE spectrum of the radical anion. ^aThe *D*_{3h} geometry is not a stationary state for ³E^{•-} on the triplet potential energy surface, so the energies for this state do not contain ZPVE corrections.

obtain reliable computed values of EA and ΔE_{ST} , we performed high-level calculations on the lowest doublet state of $(\text{CO})_3^{\bullet-}$ and on the lowest singlet and triplet states of $(\text{CO})_3$. The (U)CCSD(T)/aug-cc-pVTZ geometries and the (U)CCSD(T)/aug-cc-pVQZ energies of these states are given in Table 1, where comparisons with the experimental values of EA and ΔE_{ST} are also made.

In the $(\text{CO})_3^{\bullet-}$ radical anion, the e' σ MOs in Figure 1 are both doubly occupied, and the unpaired electron occupies the a_2'' MO. This orbital occupancy is denoted as $(e')^4(a_2'')^1$ in Table 1. The resulting ${}^2A_2''$ state of $(\text{CO})_3^{\bullet-}$ is calculated to have an optimized geometry that has D_{3h} symmetry and is an energy minimum.

Detaching the unpaired electron from the a_2'' MO in the ${}^2A_2''$ state of $(\text{CO})_3^{\bullet-}$ generates the $(e')^4(a_2'')^0$ closed-shell singlet state of neutral $(\text{CO})_3$. The geometry of this ${}^1A_1'$ singlet state, like that of the ${}^2A_2''$ state of $(\text{CO})_3^{\bullet-}$, can be optimized in D_{3h} symmetry. Since, as shown in Figure 1, the a_2'' MO is π bonding between the carbons of the three-membered ring and π antibonding between the carbons and the oxygens, removing the electron from this singly occupied MO in $(\text{CO})_3^{\bullet-}$ lengthens the C–C bonds and shortens C–O bonds. Indeed, as shown in Table 1, on going from the ${}^2A_2''$ state of $(\text{CO})_3^{\bullet-}$ to the ${}^1A_1'$ state of $(\text{CO})_3$, the C–C distances increase from 1.489 to 1.634 Å and the C–O distances decrease from 1.238 to 1.184 Å.

The EBE of the ${}^1A_1'$ state of $(\text{CO})_3$ is calculated to be 3.04 eV, a value falling well within the lower range of the experimental estimate of EA = 3.1 ± 0.1 eV. The good correspondence between the calculated EBE of the ${}^1A_1'$ state of $(\text{CO})_3$ and the experimental value gives us confidence in identifying the ${}^1A_1'$ state as the lowest energy state in the NIPE spectrum and, hence, the ground state of $(\text{CO})_3$.

However, as was found by our previous calculations,^{2c} the optimized D_{3h} geometry of the ${}^1A_1'$ state of $(\text{CO})_3$ is calculated not to be an energy minimum, but a hilltop, with two equivalent imaginary frequencies. The two imaginary frequencies correspond to degenerate, out-of-plane, e'' vibrations of the CO units, which mix the occupied e' MOs with the empty a_2'' MO in the lowest singlet state. These out-of-plane vibrations lead to the barrierless fragmentation of singlet $(\text{CO})_3$ into three molecules of CO.

Due to the dissociative nature of the ${}^1A_1'$ state of $(\text{CO})_3$ under the influence of e'' vibrations, the D_{3h} geometry of the ${}^1A_1'$ state is expected to be very short-lived. Therefore, the broadening of the band for the formation of the ${}^1A_1'$ state of $(\text{CO})_3$, which is apparent in Figure 4, can be at least partially attributed to uncertainty broadening, caused by the very short lifetime of this state.

Removal of an electron from one of the two degenerate e' MOs in the ${}^2A_2''$ state of $(\text{CO})_3^{\bullet-}$ leads to electronic states of $(\text{CO})_3$ with an $(e')^3(a_2'')^1$ electronic configuration. If the spins of the two, unpaired, σ and π electrons are parallel, then the triplet state formed is ${}^3E''$. It is expected to be considerably lower in energy than the open-shell ${}^1E''$ state that has the same orbital occupancy, but in which the spins of the unpaired electrons are antiparallel.²⁸

As shown in Table 1, our calculations find that the D_{3h} ${}^3E''$ state of $(\text{CO})_3$ is 26.9 kcal/mol higher in energy than the ${}^1A_1'$ state at the (U)CCSD(T)/aug-cc-pVQZ// (U)CCSD(T)/aug-cc-pVTZ level. This value is in good agreement with the value of $\Delta E_{\text{ST}} = -26.5$ kcal/mol obtained at the optimized D_{3h}

geometries of these two states by our previous (U)CCSD(T) calculations with the smaller 6-311+G(2df) basis set.^{2c}

However, the D_{3h} geometry of the ${}^3E''$ state is unstable toward first-order Jahn–Teller distortion. Therefore, unlike the ${}^1A_1'$ state, for which the optimized D_{3h} geometry is a hilltop on the global energy surface for the lowest singlet state, a D_{3h} geometry is not even a stationary point on the potential energy surface for the lowest triplet state. Therefore, the optimized D_{3h} geometry of the ${}^3E''$ state was not accessed by our NIPES experiments.

The stationary points on the potential energy surface for the lowest energy triplet state of $(\text{CO})_3$ are the two types of Jahn–Teller-distorted C_{2v} geometries, shown in Table 1. The orbital occupancy of the 3B_1 component of the ${}^3E''$ state is $(a_1)^1(b_2)^2(b_1)^1$, where, as shown in Figure 1, a_1 and b_2 are the C_{2v} designations for the degenerate e' σ MOs in D_{3h} $(\text{CO})_3$ and the b_1 MO in C_{2v} symmetry corresponds to the a_2'' MO of D_{3h} $(\text{CO})_3$. The orbital occupancy of the 3B_1 component of the ${}^3E''$ state gives this triplet state an optimized geometry with one long and two short C–C bonds. The orbital occupancy of the 3A_2 component of the ${}^3E''$ state is $(a_1)^2(b_2)^1(b_1)^1$, which gives this triplet state an optimized geometry with one short and two long C–C bonds.

The 2.154 Å length of the unique C–C bond in the 3B_1 state is so large that this one-electron, C–C bond is almost broken. The accompanying relief of strain in the three-membered $(\text{CO})_3$ ring results in the 3B_1 state, at its optimized C_{2v} geometry, being computed to be 22.5 kcal/mol lower in energy than the ${}^3E''$ state, at its optimized D_{3h} geometry. The Jahn–Teller distortion that involves shortening one C–C bond and lengthening two is less effective at lowering the energy of the 3A_2 component of the ${}^3E''$ state, reducing the energy of 3A_2 by only 13.1 kcal/mol at its optimized C_{2v} geometry.

The EBEs of the 3B_1 and 3A_2 states are computed to be, respectively, 3.24 and 3.64 eV. The calculated EBE of the 3A_2 state is very close to the experimental value of EBE $\approx 3.7 \pm 0.1$ eV for the onset of the band that is assigned to the second electronic state of $(\text{CO})_3$ in the 266 nm NIPE spectrum of $(\text{CO})_3^{\bullet-}$. The good agreement between the experimental EBE of the second state and the calculated EBE of the 3A_2 state, suggests that the second state of $(\text{CO})_3$ in the NIPE spectrum of $(\text{CO})_3^{\bullet-}$ is likely to be the 3A_2 triplet state.

Our calculations found that, while the 3B_1 state of $(\text{CO})_3$ is an energy minimum at its optimized C_{2v} geometry, the 3A_2 state is not a minimum but a transition structure. In the 3A_2 state, the transition state vector is an in-plane, antisymmetric, C–C stretching mode that reduces the molecular symmetry to C_s and, if followed, leads to the optimized C_{2v} geometry of the 3B_1 state of $(\text{CO})_3$. Therefore, as expected, the 3A_2 state is, indeed, the transition structure that connects two 3B_1 minima on the triplet potential energy surface for pseudorotation about the conical intersection, which occurs at D_{3h} geometries.

Since the 3A_2 state is a transition structure on the triplet potential energy surface, it is easy to explain why a very broad band is seen in the NIPE spectrum at an energy (ca. 3.7 eV) that is calculated to correspond to formation of this component of the Jahn–Teller distorted ${}^3E''$ state. However, why does an equally intense band, around the energy (3.2 eV) that is calculated for formation of the 3B_1 component of the ${}^3E''$ state, not appear in the NIPE spectrum in Figure 4? Instead, in this region of the NIPE spectrum of $(\text{CO})_3^{\bullet-}$, only a less intense

band, tentatively assigned to formation of the $^1A_1'$ hilltop, is observed.

If 3B_1 undergoes barrierless fragmentation to $^3(CO)_2 + CO$, it is possible that the 3B_1 component of the $^3E''$ state is very short-lived and thus gives rise to a very broad band in the NIPE spectrum of $(CO)_3^{\bullet-}$. However, both (U)B3LYP/6-31G(d) and (U)CCSD(T)/aug-cc-pVTZ vibrational analyses show that, unlike 3A_2 , 3B_1 is an energy minimum, not a transition structure. Therefore, an energy barrier is predicted to separate 3B_1 from $^3(CO)_2 + CO$.

As depicted schematically in Figure 5, there appear actually to be two transition states that 3B_1 must cross, in order to

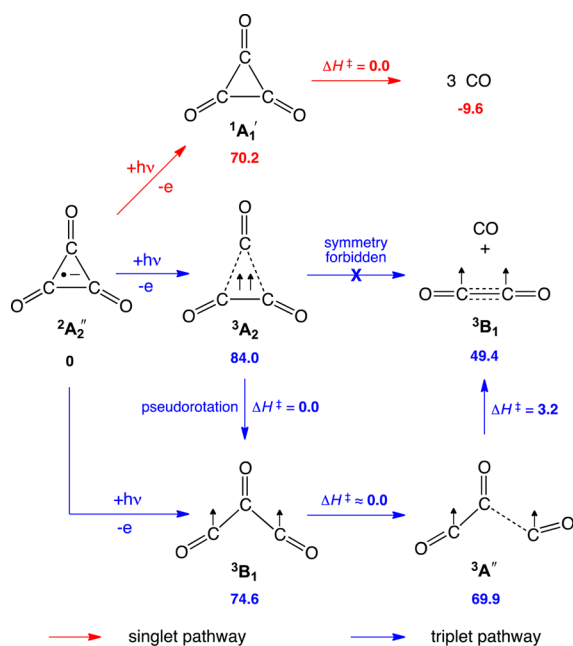


Figure 5. Pathways for $(CO)_3$ fragmentation on the singlet (red arrows) and the triplet (blue arrows) potential energy surfaces. The number at the bottom of each structure is its (U)CCSD(T)/aug-cc-pVQZ//[(U)CCSD(T)/aug-cc-pVTZ energy in kcal/mol, relative to that of the radical anion, with zero-point vibrational energy corrections included.

undergo fragmentation. The first involves antisymmetric C–C bond length and O–C–C angle distortions, which lead to a $^3A''$ intermediate with only C_s symmetry. The transition structure for this step is only 0.1 kcal/mol higher in energy than the 3B_1 structure. Since the $^3A''$ state is calculated to be 4.7 kcal/mol lower in energy than the 3B_1 state, conversion of the C_{2v} geometry of 3B_1 to the C_s geometry of $^3A''$ must be nearly barrierless.²⁹

The second step in the fragmentation of 3B_1 involves cleavage of the longer C–C bond in the C_s geometry of the $^3A''$ state of $(CO)_3$, forming $^3(CO)_2 + CO$. The calculated barrier to this step of $\Delta H^\ddagger = 3.2$ kcal/mol, places the transition state for it $3.2\text{--}4.7 = -1.5$ kcal/mol below the energy of 3B_1 . Therefore, our calculations indicate that, although 3B_1 may be an energy minimum, the barrier to its fragmentation to $^3(CO)_2 + CO$ must be very small.

Even if the 3B_1 component of the $^3E''$ state were a transition structure on the global, triplet $(CO)_3$ potential energy surface, its formation should give rise to a large, broad band around 3.2 eV in the NIPE spectrum of $(CO)_3^{\bullet-}$. Consequently, the absence from the NIPE spectra in Figure 4 of either sharp peaks

or a broad band, attributable to the 3B_1 component of $^3E''$, is puzzling, especially since there does appear to be a broad band in the spectra for formation of 3A_2 component of the $^3E''$ state.

However, there is, possibly, a simple explanation for the absence of a band for formation of the 3B_1 state. It is conceivable that the FCFs²⁶ for formation of the C_{2v} geometry of the 3B_1 state, with its one extremely long C–C bond, are much smaller than the FCFs for formation of the less geometrically distorted 3A_2 state. In order to test this hypothesis, we computed the FCFs for formation of both the 3B_1 and 3A_2 states²⁸ of $(CO)_3$ and also for formation of the $^1A_1'$ ground state from the $^2A_2''$ state of $(CO)_3^{\bullet-}$.

Franck–Condon Simulations of the Vibrational Structure in the NIPE Spectrum. The vibrational bands, simulated from the FCFs for the formation of the $^1A_1'$ and 3A_2 states of neutral $(CO)_3$ from the $^2A_2''$ ground state of $(CO)_3^{\bullet-}$, are given in Figure 6. In this figure they are compared with the broad bands, observed in the 266 nm NIPE spectrum and assigned to these two states.

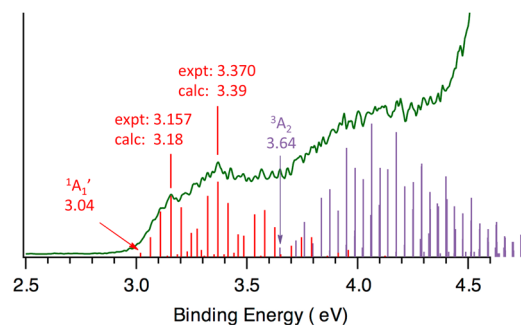


Figure 6. Simulated NIPE spectrum of $(CO)_3^{\bullet-}$, superimposed on the experimental 266 nm spectrum. In order to match the two maxima at EBE = 3.157 and 3.370 eV in the experimental spectrum, the simulated 0–0 band for formation of the $^1A_1'$ electronic state of $(CO)_3$ has been positioned at EBE = 3.02, 0.02 eV = 0.5 kcal/mol lower than the computed value. The position of the simulated 0–0 band for formation of the 3A_2 electronic state of $(CO)_3$ has not been adjusted. The relative amplitudes of the vibrational lines for formation of each electronic state are those computed from the FCFs. Only the relative amplitudes of the vibrational progressions in the two different electronic states have been adjusted to match the peak heights in the experimental spectrum.

We also simulated the vibrational bands for formation of the 3B_1 state. However, the vibrational wave function of the $^2A_2''$ state of $(CO)_3^{\bullet-}$ is calculated to have no overlap with the vibrational wave function for the 3B_1 state of neutral $(CO)_3$. The very large change in geometry on going from the $^2A_2''$ state to the 3B_1 state, which involves the lengthening of one C–C bond by more than 0.6 Å, accounts for the fact that the vibrational wave functions for these two states do not have any overlap. The lack of overlap between the vibrational wave functions for these two states means that all of the FCFs for the $^2A_2'' \rightarrow ^3B_1$ transition are zero, and this explains why this transition apparently has no intensity in the NIPE spectrum of $(CO)_3^{\bullet-}$.

As shown in Figure 6, the simulated vibrational progressions for formation of the $^1A_1'$ and 3A_2 states of $(CO)_3$ provide a very good fit, up to about 4.0 eV, to the shapes of the broad bands in the experimental NIPE spectrum. Our simulation duplicates the existence of the two small maxima within the $^1A_1'$ manifold that are visible in the experimental spectrum. The positions of these

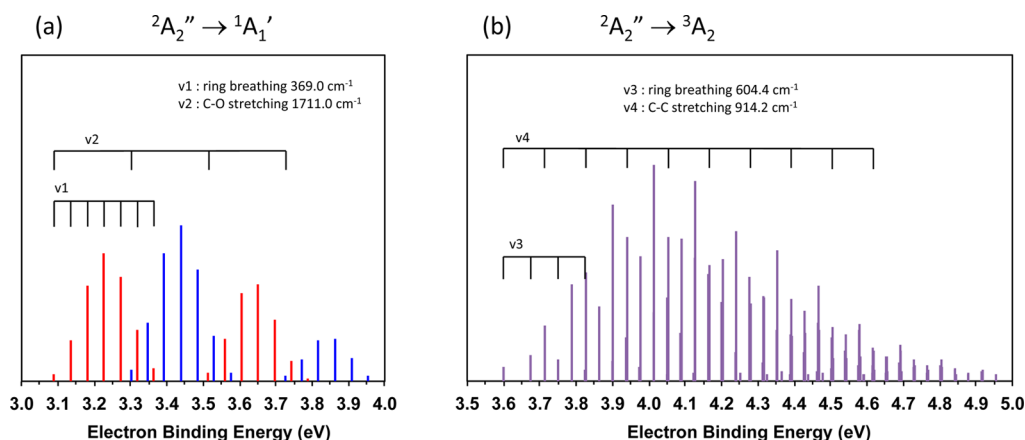


Figure 7. Assignments of the vibrational peaks belonging to (a) the ${}^1A_1'$ state and (b) the 3A_2 state of $(\text{CO})_3$ in the simulated NIPE spectrum of $(\text{CO})_3^{\bullet-}$. Note that the simulated vibrational bands for formation of the 3A_2 state extend up to EBE = 5.0 eV. However, in the experimental spectrum, the upper limit of the EBE that can be accessed with the 266 nm laser is only 4.6 eV, and the peaks above about 4.4 eV are obscured by the large, rising tail that appears to begin at this EBE.

maxima are calculated to be at EBE = 3.18 and 3.39 eV. Both of these EBEs are about 0.02 eV larger than the observed positions of these maxima at EBE = 3.157 and 3.370 eV in the experimental NIPE spectrum.

The simulated NIPE spectrum, shown in Figure 6, is depicted in an expanded scale in Figure 7, and the vibrational progressions in the spectrum are assigned to specific vibrational modes. The vibrational progression for formation of the ${}^1A_1'$ state of $(\text{CO})_3$ consists of four groups of seven peaks; although, in the last of the four groups, only six peaks are visible. For simplicity in viewing, adjacent septets are differentiated by alternant red and blue colors.

As shown in Figure 7a, the computed spacing within each group of seven peaks is $\nu_1 = 369.0 \text{ cm}^{-1}$, which is the calculated frequency of the ring breathing vibration in the ${}^1A_1'$ state of $(\text{CO})_3$. The spacing between the septets is $\nu_2 = 1711.0 \text{ cm}^{-1}$, which is the frequency computed for the totally symmetric C=O stretching vibration in this state.

In NIPES, as in other types of electronic spectroscopy, progressions are seen in vibrational modes that affect the geometrical parameters by which the ground state (in NIPES the lowest electronic state of the radical anion) and an excited state (in NIPES an electronic state of the neutral molecule) differ.^{15d,e,26,27a} In general, vibrational progressions usually increase in length as the size of the differences between the ground state and the excited state geometries increases. Thus, the long progressions in C–C and C=O stretching in Figure 7a are easily explained by the large differences between the optimized C–C and C=O bond lengths in the ${}^2A_2''$ ground state of the $(\text{CO})_3^{\bullet-}$ radical anion and in the ${}^1A_1'$ ground state of neutral $(\text{CO})_3$.

As shown in Table 1, detachment of the electron from the a_2'' MO in the radical anion results in the calculated C–C bond lengths increasing by 0.145 Å and the C–O bond lengths decreasing by 0.054 Å. As discussed in the previous section, these changes in bond lengths can easily be understood by the changes in bonding that occur upon removal of the electron that occupies the a_2'' MO in $(\text{CO})_3^{\bullet-}$.

According to the assignments of the vibrational peaks in the simulation in Figure 7a, the two maxima at EBE = 3.157 ± 0.005 and 3.370 ± 0.005 eV in the experimental NIPE spectrum in Figure 6 each contain three quanta of the vibrational energy for ring breathing but differ by one quantum

in the vibrational energy for C=O stretching. Thus, the C=O stretching frequency at the hilltop for the concerted fragmentation of the singlet ground state of $(\text{CO})_3$ to three molecules of CO is equal to the energy difference between these two maxima of $0.213 \pm 0.007 \text{ eV} = 1720 \pm 60 \text{ cm}^{-1}$. Our calculated value for the C=O stretching frequency at the ${}^1A_1'$ hilltop is 1711 cm^{-1} , in excellent agreement with the experimentally measured value.

The simulated vibrational structure for the formation of the 3A_2 state is also shown in Figures 6 and 7b. Two C–C stretching and one C=O stretching modes contribute to the vibrational structure in the ${}^2A_2'' \rightarrow {}^3A_2$ transition. However, the progressions of the sole C=O stretching mode are so weak that they are hardly visible above the baseline, and they are only visible when coupled with the C–C stretching modes. The two C–C stretching modes (ν_3 and ν_4) that contribute to most of the vibrational structure in the ${}^2A_2'' \rightarrow {}^3A_2$ transition have computed frequencies of 604.4 and 914.2 cm^{-1} .

The lower frequency vibration involves stretching of all three C–C bonds with the same phase, so it can be termed a ring breathing mode. The higher frequency vibration involves stretching the one unique C–C bond and shortening the two equivalent C–C bonds.

The first of these two modes is active in the ${}^2A_2'' \rightarrow {}^3A_2$ transition, because the average C–C bond length of 1.548 Å in the 3A_2 state is 0.059 Å longer than in the ${}^2A_2''$ state. The second mode is active in this laser-induced electronic transition because the deviations of the individual C–C bond lengths in the 3A_2 state from the average C–C bond length in this state are 0.070 Å for the two equivalent bonds and -0.141 Å for the unique C–C bond. In contrast, since the geometry of the ${}^2A_2''$ state has D_{3h} symmetry, the deviation of the individual C–C bond lengths from the average C–C bond length in this state is, of course, zero.

The 3A_2 state of $(\text{CO})_3$ does not have D_{3h} symmetry, because this state is, of course, actually one component of the ${}^3E''$ state of $(\text{CO})_3$; and an e' distortion from D_{3h} symmetry stabilizes the ${}^3E''$ state via a first-order Jahn–Teller effect.¹² The e' distortion of the C–C bond lengths results in the unique C–C bond in the C_{2v} optimized geometry of 3A_2 being shorter than the average of C–C bond lengths by about twice the amount by which the two equivalent C–C bonds are longer than the average. Therefore, 914.2 cm^{-1} is the frequency of the vibration

that takes the optimized C_{2v} geometry of the 3A_2 state back toward the D_{3h} geometry of the undistorted ${}^3E''$ state.³⁰

Unfortunately, the very short lifetime of the 3A_2 state of $(CO)_3$, before it pseudorotates from C_{2v} symmetry toward the geometry of the 3B_1 energy minima, broadens the band in the NIPE spectrum for formation of the 3A_2 state. Consequently, the calculated frequency of 914.2 cm^{-1} for the vibration that takes the optimized C_{2v} geometry of the 3A_2 state of $(CO)_3$ back toward the D_{3h} geometry of the undistorted ${}^3E''$ state cannot be compared with the experimental value for this vibrational frequency. However, the calculated frequency of 914.2 cm^{-1} can be compared with the observed frequency of $1050 \pm 40\text{ cm}^{-1}$ (calculated 1028 cm^{-1}) for the same type of vibration that takes the C_{2v} Jahn–Teller-distorted geometry of the lowest triplet state of $(CO)_3$ back toward the undistorted D_{3h} geometry of the ${}^3E_2''$ state.⁴

As shown in Figures 6 and 7, the photodetachment transitions of ${}^2A_2''$ of $(CO)_3^{\bullet-} \rightarrow {}^1A_1'$ and 3A_2 of $(CO)_3$ are calculated to be accompanied by a dense set of vibrational excitations. These excitations could contribute to the breadth of the bands that are seen in the experimental NIPE spectra in Figures 4 and 6. However, as discussed above, it is tempting to ascribe the principal cause of spectral broadening to the short lifetimes expected for the ${}^1A_1'$ and 3A_2 states of $(CO)_3$.

In order to estimate the contribution of lifetime broadening to the NIPE spectrum of $(CO)_3^{\bullet-}$, we convoluted the stick spectrum in Figure 6, using Gaussian line shapes of different fwhm. For each vibrational transition, full widths at half-maxima (fwhm) values of 30, 40, 50, 70, and 100 meV were used to generate a series of simulated NIPE spectra, which are shown in Figure 8.

The spectrum, simulated with fwhm = 40 meV, shows a well-resolved C=O stretching progression for the singlet transition. However, the experimental spectrum, which was taken with an instrumental resolution of ca. 45 meV fwhm for the singlet state region, looks more like the NIPE spectrum that was simulated with Gaussian line widths of fwhm=70 meV. This implies ca. 25 meV (200 cm^{-1}) of additional broadening in the singlet state region. Assuming that this broadening is due to the short lifetime of the ${}^1A_1'$ state of $(CO)_3$ leads to an estimated lifetime of about $\Delta t = \hbar/2\pi\Delta E = 25\text{ fs}$ for this singlet state.

The experimental spectral feature, corresponding to the triplet state of $(CO)_3$, was measured with a 30 meV fwhm instrumental resolution, which, as shown in Figure 8, would give rise to a nicely resolved vibrational structure, if the 3A_2 state of $(CO)_3$ were long-lived. The fact that there is no vibrational structure observed in the experimental NIPE spectrum for the transition to the triplet state and that Gaussians with line widths of 50 meV fwhm start to smooth out the vibrational features in the simulation, suggests an extra broadening of ca. 20 meV (150 cm^{-1}). If this broadening is ascribed to the short-lived nature of the 3A_2 state, its lifetime can be estimated from the uncertainty principle to be about $\Delta t = \hbar/2\pi\Delta E = 35\text{ fs}$.

SUMMARY AND CONCLUSIONS

NIPE spectra of the radical anion of cyclopropane-1,2,3-trione, $(CO)_3^{\bullet-}$, have been obtained at 20 K, using both 355 and 266 nm lasers for electron photodetachment. Due to the short lifetimes of both the ${}^1A_1'$ and 3A_2 states of $(CO)_3$ that are formed by electron detachment from $(CO)_3^{\bullet-}$ and, to a lesser extent, to the vibrational progressions that accompany the photodetachment process, the NIPE spectra of $(CO)_3^{\bullet-}$ show

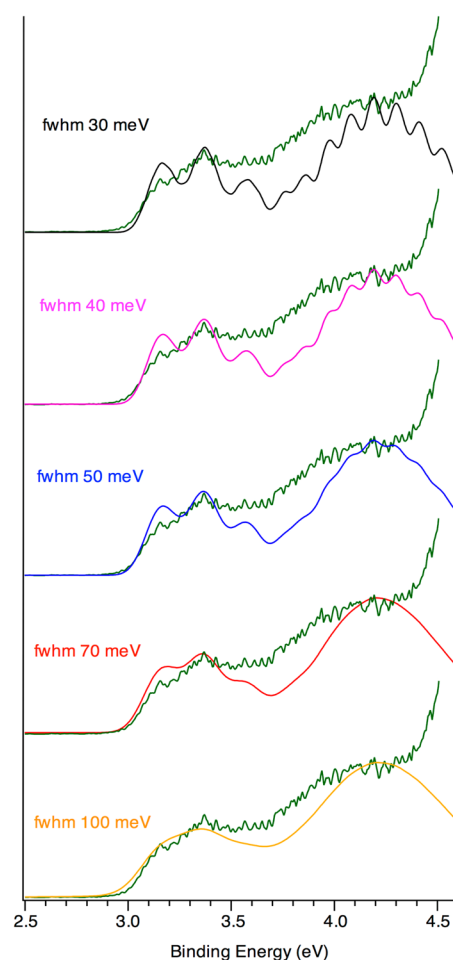


Figure 8. Stick spectrum in Figure 6, convoluted using Gaussian line shapes with full widths at half maxima of 30 (black), 40 (magenta), 50 (blue), 70 (red), and 100 meV (orange), superimposed on the experimental 266 nm spectrum (green). The convoluted spectra were obtained by multiplying the Gaussians by the FCFs for the singlet and 2.5 times the FCFs for the triplet and summing.

very broad bands. The smaller intensity of the band with EBE = $3.1 \pm 0.1\text{ eV}$ than of the band with EBE = $3.7 \pm 0.1\text{ eV}$ in the 266 nm NIPE spectrum suggests that the singlet is the ground state of $(CO)_3$. From the NIPE spectrum the EA and the singlet–triplet energy gap of $(CO)_3$ are estimated to be, respectively, EA = $3.1 \pm 0.1\text{ eV}$ and $\Delta E_{ST} = -14 \pm 3\text{ kcal/mol}$.

By performing high-level (U)CCSD(T)/aug-cc-pVQZ// (U)CCSD(T)/aug-cc-pVTZ calculations, we obtained EA = 3.04 eV for the ${}^1A_1'$ singlet state of $(CO)_3$ and $\Delta E_{ST} = -13.8\text{ kcal/mol}$ for the energy difference between ${}^1A_1'$ and 3A_2 states of $(CO)_3$. These calculated values are in excellent agreement with the experimental values.

Vibrational analyses find that the optimized D_{3h} geometry of the ${}^1A_1'$ state of $(CO)_3$ is a hilltop for concerted fragmentation to three molecules of CO on the singlet potential energy surface, and the 3A_2 component of ${}^3E''$ is a transition structure for the pseudorotation about the Jahn–Teller cone that connects the two adjacent 3B_1 minima.

These two barrierless reactions, fragmentation of the ${}^1A_1'$ hilltop to three molecules of CO and pseudorotation of the 3A_2 transition state to a 3B_1 energy minimum, predict that both of these electronic states will have very short lifetimes. The short lifetimes expected for ${}^1A_1'$ and 3A_2 are the main contributors to

the very broad widths of the bands for the formation of these two states in the NIPE spectra of $(\text{CO})_3^{\bullet-}$.

Our simulations of the vibrational progressions, calculated for formation of the ${}^1\text{A}_1'$ and ${}^3\text{A}_2$ states of $(\text{CO})_3$ from the ${}^2\text{A}_2''$ state of $(\text{CO})_3^{\bullet-}$, provide very good fits to the shapes of the broad bands that are assigned to formation of these two states of $(\text{CO})_3$ in the 266 nm NIPE spectra. Our calculations of FCFs also explain the reason why no band, corresponding to the formation of the ${}^3\text{B}_1$ component of ${}^3\text{E}''$, is seen in the spectrum. The vibrational wave function for the ${}^2\text{A}_2''$ state of $(\text{CO})_3^{\bullet-}$ at its D_{3h} geometry is calculated to have no Franck–Condon overlap with the vibrational wave function for the ${}^3\text{B}_1$ state of $(\text{CO})_3$ at its highly distorted C_{2v} geometry. Therefore, the ${}^2\text{A}_2'' \rightarrow {}^3\text{B}_1$ transition has no intensity in the NIPE spectra of $(\text{CO})_3^{\bullet-}$.

The NIPE spectra of $(\text{CO})_3^{\bullet-}$, along with their calculation-assisted interpretation, confirm the two previously made predictions that the ground state of $(\text{CO})_3$ is a singlet and that this state undergoes barrierless fragmentation to three molecules of CO. In addition, the spectra demonstrate that NIPES can not only access and provide information about transition structures¹⁵ but can also access and provide information about hilltops on potential energy surfaces. For example, the assignment of the two peaks at $\text{EBE} = 3.157 \pm 0.005$ and 3.370 ± 0.005 eV in the ${}^1\text{A}_1'$ region of the NIPE spectrum establishes that the C=O stretching frequency at the D_{3h} hilltop on the ${}^1\text{A}_1'$ potential energy surface is 1720 ± 60 cm^{-1} (calculated 1711.0 cm^{-1}). To the best of our knowledge, this is the first measurement of a vibrational frequency at a hilltop on a potential energy surface.

■ ASSOCIATED CONTENT

■ Supporting Information

The calculated FCFs used to simulate the NIPE stick spectrum of $(\text{CO})_3^{\bullet-}$, the simulated NIPES spectrum of $(\text{CO})_3^{\bullet-}$, using the (U)B3LYP/6-31G(d) FCFs for the formation of $(\text{CO})_3$ from $(\text{CO})_3^{\bullet-}$, the results of (U)B3LYP/6-31G(d) and (12/9)CASPT2/aug-cc-pVTZ calculations of the geometries and energies of the low-lying electronic states of $(\text{CO})_3^{\bullet-}$ and $(\text{CO})_3$, and the (U)CCSD(T)/aug-cc-pVTZ optimized geometries and (U)CCSD(T)/aug-cc-pVQZ energies in hartrees for the ${}^2\text{A}_2''$ ground state of $(\text{CO})_3^{\bullet-}$ and for the ${}^1\text{A}_1'$, ${}^3\text{E}''$, ${}^3\text{A}_2$, ${}^3\text{B}_1$, and ${}^3\text{A}''$ states of $(\text{CO})_3$. This material is available free of charge via the Internet at <http://pubs.acs.org>.

■ AUTHOR INFORMATION

Corresponding Authors

xuebin.wang@pnnl.gov
weston.borden@unt.edu

Notes

The authors declare no competing financial interest.

■ ACKNOWLEDGMENTS

The calculations at UNT were supported by grant CHE-0910527 from the National Science Foundation and grant B0027 from the Robert A. Welch Foundation. The NIPES research at PNNL was supported by the U.S. Department of Energy (DOE), Office of Basic Energy Sciences, Division of Chemical Sciences, Geosciences and Biosciences (X.-B.W.) and was performed at the EMSL, a national scientific user facility sponsored by DOE's Office of Biological and Environmental Research and located at Pacific Northwest National Laboratory.

■ REFERENCES

- (a) Gleiter, R.; Hyla-Kryspin, I.; Pfeifer, K.-H. *J. Org. Chem.* **1995**, *60*, 5878. (b) Jiao, H.; Frapper, G.; Halet, J.-F.; Saillard, J.-Y. *J. Phys. Chem. A* **2001**, *105*, 5945. (c) For some very recently published computational studies on $(\text{CO})_4$, see Perera, A.; Molt, R. W., Jr.; Lotrich, V. F.; Bartlett, R. J. *Theor. Chem. Acc.* **2014**, *133*, 1514.
- (a) Zhou, X.; Hrovat, D. A.; Gleiter, R.; Borden, W. T. *Mol. Phys.* **2009**, *107*, 863. (b) Zhou, X.; Hrovat, D. A.; Borden, W. T. *J. Phys. Chem. A* **2010**, *114*, 1304. (c) Bao, X.; Zhou, X.; Lovitt, C. F.; Venkatraman, A.; Hrovat, D. A.; Gleiter, R.; Hoffmann, R.; Borden, W. T. *J. Am. Chem. Soc.* **2012**, *134*, 10259.
- (a) Guo, J.-C.; Hou, G.-L.; Li, S. D.; Wang, X.-B. *J. Phys. Chem. Lett.* **2012**, *3*, 304.
- (a) For our previous NIPE spectroscopy study on $(\text{CO})_5^{\bullet-}$ and $(\text{CO})_6^{\bullet-}$, see: Bao, X.; Hrovat, D. A.; Borden, W. T.; Wang, X. B. *J. Am. Chem. Soc.* **2013**, *135*, 4291. (b) A species with the formula of $\text{C}_6\text{O}_6^{\bullet-}$ has been reported to be formed by oligomerization of CO on molybdenum anions: Wyrwas, R. B.; Jarrold, C. C. *J. Am. Chem. Soc.* **2006**, *128*, 13688. However, a NIPE spectrum of this anion gave $\text{EA} = 2.5$ eV, which is 1.2 eV smaller than the EA of the radical anion of 1,2,3,4,5,6-cyclohexanhexone, $(\text{CO})_6^{\bullet-}$, reported by us.^{4a} Therefore, it appears that the $\text{C}_6\text{O}_6^{\bullet-}$, generated by Wyrwas and Jarrold, has a different structure from the $(\text{CO})_6^{\bullet-}$ prepared by us.
- (a) Bao, X.; Hrovat, D. A.; Borden, W. T. *Chem.—Eur. J.* **2013**, *19*, 5687. (b) Zhang, J.; Hrovat, D. A.; Sun, Z.; Bao, X.; Borden, W. T.; Wang, X.-B. *J. Phys. Chem. A* **2013**, *117*, 7841.
- (a) Fort, R. C., Jr.; Getty, S. J.; Hrovat, D. A.; Lahti, P. M.; Borden, W. T. *J. Am. Chem. Soc.* **1992**, *114*, 7549. (b) Chen, B.; Hrovat, D. A.; Deng, S. H. M.; Zhang, J.; Wang, X.-B.; Borden, W. T. *J. Am. Chem. Soc.* **2014**, *136*, 3589.
- (a) Farnell, L.; Radom, L.; Vincent, M. A. *J. Mol. Struct. (THEOCHEM)* **1981**, *76*, 1. (b) Herndon, W. C. *J. Mol. Struct. (THEOCHEM)* **1983**, *103*, 219. (c) Evangelisti, S. *Chem. Phys.* **1997**, *218*, 21. (d) Sabzyan, H.; Noorbala, M. R. *J. Mol. Struct. (THEOCHEM)* **2003**, *626*, 143. (e) Corkran, G.; Ball, D. W. *J. Mol. Struct. (THEOCHEM)* **2004**, *668*, 171. (f) Sahu, P. K.; Lee, S.-L. *Int. J. Quantum Chem.* **2005**, *103*, 314.
- Deltic acid, $(\text{CO})_3\text{H}_2$, is found to dissociate readily to the dianion of $(\text{CO})_3$, $(\text{CO})_3^{2-}$, presumably because the dianion possesses 2π aromaticity.^{7b,10,11}
- West, R. *Oxocarbons*; Academic Press: New York, 1980.
- (a) Aihara, J.-I. *J. Am. Chem. Soc.* **1981**, *103*, 1633. (b) Schleyer, P. v. R.; Najafian, K.; Kiran, B.; Jiao, H. *J. Org. Chem.* **2000**, *65*, 426. (c) Domene, C.; Fowler, P. W.; Jenkens, L. W.; Steiner, E. *Chem.—Eur. J.* **2007**, *13*, 269.
- (11) With MOs that are topologically similar to those of $(\text{CO})_3^{2-}$, $\text{P}_3\text{F}_9^{2-}$ is also found to be 2π aromatic. See: Priyakumari, C. P.; Jemmis, E. D. *J. Am. Chem. Soc.* **2013**, *135*, 16026.
- (a) Jahn, H. A.; Teller, E. *Proc. R. Soc. London A* **1937**, *161*, 220. (b) Davidson, E. R.; Borden, W. T. *J. Phys. Chem.* **1983**, *87*, 4783. (c) Bersuker, I. B. *The Jahn-Teller Effect*; Cambridge University Press: Cambridge, U.K., 2006.
- (a) Hirst, D. M.; Hopton, J. D.; Linnett, J. W. *Tetrahedron Suppl.* **1963**, *2*, 15. (b) Glmarc, B. M. *J. Am. Chem. Soc.* **1970**, *92*, 266. (c) Bodor, N.; Dewar, M. J. S.; Harget, A.; Haselbach, E. *J. Am. Chem. Soc.* **1970**, *92*, 3854. (d) Haddon, R. C. *Tetrahedron Lett.* **1972**, *13*, 3897. (e) Fleischhauer, J.; Beckers, M.; Scharf, H.-D. *Tetrahedron Lett.* **1973**, *14*, 4275. (f) Beebe, N. H. F.; Sabin, J. R. *Chem. Phys. Lett.* **1974**, *24*, 389. (g) Haddon, R. C.; Poppinger, D.; Radom, L. *J. Am. Chem. Soc.* **1975**, *97*, 1645. (h) Raine, G. P.; Schaefer, H. F., III; Haddon, R. C. *J. Am. Chem. Soc.* **1983**, *105*, 194. (i) Frenking, G. *Angew. Chem., Int. Ed. Engl.* **1990**, *29*, 1410. (j) Janoschek, R. *J. Mol. Struct.* **1991**, *232*, 147. (k) Korin, A. A.; Balkova, A.; Bartlett, R. J.; Boyd, R. J.; Schleyer, P. v. R. *J. Phys. Chem.* **1996**, *100*, 5702. (l) Schröder, D.; Heinemann, C.; Schwarz, H.; Harvey, J. N.; Dua, S.; Blanksby, S. J.; Bowie, J. H. *Chem.—Eur. J.* **1998**, *4*, 2550. (m) Talbi, D.; Chandler, G. S. *J. Phys. Chem. A* **2000**, *104*, 5872. (n) Wang, H.-Y.; Lu, X.; Huang, R.-B.; Zheng, L.-S. *J. Mol. Struct.* **2002**, *593*, 187. (o) Trindle, C. *Int. J. Quantum Chem.* **2003**, *93*, 286. (p) Maclagan, R. G. A. R. *J. Mol. Struct.*

2005, 713, 107. (q) Golovin, A. V.; Ponomarev, D. A.; Takhistov, V. V. *J. Comput. Methods Mol. Des.* **2011**, *1*, 14.

(14) (a) Woodward, R. B.; Hoffmann, R. *Angew. Chem., Int. Ed.* **1969**, *8*, 781. (b) Woodward, R. B.; Hoffmann, R. *The Conservation of Orbital Symmetry*; Academic Press: New York, 1970.

(15) For a review, see: (a) Neumark, D. M. *Acc. Chem. Res.* **1993**, *26*, 33. For original papers, see: (b) Wenthold, P. G.; Hrovat, D. A.; Borden, W. T.; Lineberger, W. C. *Science* **1996**, *272*, 1456. (c) Neumark, D. M. *Phys. Chem. Chem. Phys.* **2005**, *7*, 433. (d) Ichino, T.; Villano, S. M.; Gianola, A. J.; Goebbert, D. J.; Velarde, L.; Sanov, A.; Blanksby, S. J.; Zhou, X.; Hrovat, D. A.; Borden, W. T.; Lineberger, W. C. *Angew. Chem., Int. Ed.* **2009**, *48*, 8509. (e) Ichino, T.; Villano, S. M.; Gianola, A. J.; Goebbert, D. J.; Velarde, L.; Sanov, A.; Blanksby, S. J.; Zhou, X.; Hrovat, D. A.; Borden, W. T.; Lineberger, W. C. *J. Phys. Chem. A* **2011**, *115*, 1634. (f) Westermann, T.; Kin, J. B.; Weichman, M. L.; Hock, C.; Yacovitch, T. I.; Palma, J.; Neumark, D. M.; Manthe, U. *Angew. Chem., Int. Ed.* **2014**, *53*, 1122.

(16) Wang, X. B.; Wang, L. S. *Rev. Sci. Instrum.* **2008**, *79*, 073108.

(17) (a) Eggerding, D.; West, R. *J. Am. Chem. Soc.* **1975**, *97*, 207. (b) Eggerding, D.; West, R. *J. Am. Chem. Soc.* **1976**, *98*, 3641.

(18) (a) Becke, A. D. *J. Chem. Phys.* **1993**, *98*, 5648. (b) Lee, C.; Yang, W.; Parr, R. G. *Phys. Rev. B* **1988**, *37*, 785.

(19) Hariharan, P. C.; Pople, J. A. *Theoret. Chimica Acta* **1973**, *28*, 213.

(20) Frisch, M. J.; Trucks, G. W.; Schlegel, H. B.; Scuseria, G. E.; Robb, M. A.; Cheeseman, J. R.; Scalmani, G.; Barone, V.; Mennucci, B.; Petersson, G. A.; Nakatsuji, H.; Caricato, M.; Li, X.; Hratchian, H. P.; Izmaylov, A. F.; Bloino, J.; Zheng, G.; Sonnenberg, J. L.; Hada, M.; Ehara, M.; Toyota, K.; Fukuda, R.; Hasegawa, J.; Ishida, M.; Nakajima, T.; Honda, Y.; Kitao, O.; Nakai, H.; Vreven, T.; Montgomery, J. A., Jr.; Peralta, J. E.; Ogliaro, F.; Bearpark, M.; Heyd, J. J.; Brothers, E.; Kudin, K. N.; Staroverov, V. N.; Kobayashi, R.; Normand, J.; Raghavachari, K.; Rendell, A.; Burant, J. C.; Iyengar, S. S.; Tomasi, J.; Cossi, M.; Rega, N.; Millam, N. J.; Klene, M.; Knox, J. E.; Cross, J. B.; Bakken, V.; Adamo, C.; Jaramillo, J.; Gomperts, R.; Stratmann, R. E.; Yazyev, O.; Austin, A. J.; Cammi, R.; Pomelli, C.; Ochterski, J. W.; Martin, R. L.; Morokuma, K.; Zakrzewski, V. G.; Voth, G. A.; Salvador, P.; Dannenberg, J. J.; Dapprich, S.; Daniels, A. D.; Farkas, O.; Foresman, J. B.; Ortiz, J. V.; Cioslowski, J.; Fox, D. J. *Gaussian 09*, revision A.02, Gaussian, Inc.: Wallingford, CT, 2009.

(21) (a) Purvis, G. D.; Bartlett, R. J. *J. Chem. Phys.* **1982**, *76*, 1910. (b) Raghavachari, K.; Trucks, G. W.; Pople, J. A.; Head-Gordon, M. H. *Chem. Phys. Lett.* **1989**, *157*, 479.

(22) (a) Dunning, T. H., Jr. *J. Chem. Phys.* **1989**, *90*, 1007. (b) Kendall, R. A.; Dunning, T. H., Jr.; Harrison, R. J. *J. Chem. Phys.* **1992**, *96*, 6769.

(23) (a) Werner, H.-J.; Knowles, P. J.; Knizia, G.; Manby, F. R.; Schütz, M. *Comput. Mol. Sci.* **2012**, *2*, 242. (b) Werner, H.-J.; Knowles, P. J.; Knizia, G.; Manby, F. R.; Schütz, M.; Celani, P.; Korona, T.; Lindh, R.; Mitrushenkov, A.; Rauhut, G.; Shamasundar, K. R.; Adler, T. B.; Amos, R. D.; Bernhardsson, A.; Berning, A.; Cooper, D. L.; Deegan, M. J. O.; Dobbyn, A. J.; Eckert, F.; Goll, E.; Hampel, C.; Hesselmann, A.; Hetzer, G.; Hrenar, T.; Jansen, G.; Köppl, C.; Liu, Y.; Lloyd, A. W.; Mata, R. A.; May, A. J.; McNicholas, S. J.; Meyer, W.; Mura, M. E.; Nicklass, A.; O'Neill, D. P.; Palmieri, P.; Peng, D.; Pflüger, K.; Pitzer, R.; Reiher, M.; Shiozaki, T.; Stoll, H.; Stone, A. J.; Tarroni, R.; Thorsteinsson, T.; Wang, M. *MOLPRO, a package of ab initio programs*, version 2010.1; University College Cardiff Consultants Limited: Cardiff, U.K., 2010; see <http://www.molpro.net>.

(24) Mozhayskiy, V. A.; Krylov, A. I. *ezSpectrum*, version 3.0; University of Southern California: Los Angeles, CA, 2009; see <http://iopshell.usc.edu/downloads>.

(25) (a) Kupka, H.; Cribb, P. *J. Chem. Phys.* **1986**, *85*, 1303. (b) Berger, R.; Fischer, C.; Klessinger, M. *J. Phys. Chem. A* **1998**, *102*, 7157. (c) Duschinsky, F. *Acta Physicochim. USSR* **1937**, *7*, 551.

(26) (a) Franck, J. *Trans. Faraday Soc.* **1926**, *21*, 536. (b) Condon, E. *Phys. Rev.* **1926**, *28*, 1182.

(27) (a) Lineberger, W. C.; Borden, W. T. *Phys. Chem. Chem. Phys.* **2011**, *13*, 11792. (b) Clifford, E. P.; Wenthold, P. G.; Lineberger, W.

C.; Ellison, G. B.; Wang, C. X.; Grabowski, J. J.; Vila, F.; Jordan, K. D. *J. Chem. Soc., Perkin Trans. 2* **1998**, 1015.

(28) Unless the singly occupied MOs are disjoint, formation of open-shell singlet states, with the same orbital occupancies as triplet states, is expected to occur at energies that are higher than those of the triplet states. Indeed, the results of our (12/9)CASPT2/aug-cc-pVTZ calculations on the 1B_1 and 1A_2 singlet states, which are reported in the Supporting Information, predict that formation of these two singlet states should occur at EBEs that are, respectively, 0.27 and 0.33 eV higher than their corresponding 3B_1 and 3A_2 triplet states. Since, unlike triplet states, open-shell singlets have only one spin component, the bands for formation of open-shell singlet states in NIPE spectra are expected to be less intense than the bands for formation of the corresponding triplet states.²⁷

(29) 3B_1 has one more real vibrational frequency than the transition structure that connects it to $^3A''$. Therefore, with inclusion of zero-point energy corrections, 3B_1 has an energy that is actually calculated to be 1.6 kcal/mol higher than that of the transition structure.

(30) The triplet state of neutral (CO)₅ that gives rise to a vibrational progression in the NIPE spectrum of (CO)₅^{•+} is also a Jahn-Teller distorted state with a C_{2v} equilibrium geometry.⁴